Developmental Biology 407 (2015) 12–25

Contents lists available at ScienceDirect

Developmental Biology

journal homepage: www.elsevier.com/locate/developmentalbiology

VEGF signals induce trailblazer cell identity that drives neural crest migration

Rebecca McLennan [a,1], Linus J. Schumacher [b,c,1], Jason A. Morrison [a], Jessica M. Teddy [a], Dennis A. Ridenour [a], Andrew C. Box [a], Craig L. Semerad [a], Hua Li [a], William McDowell [a], David Kay [c], Philip K. Maini [b], Ruth E. Baker [b], Paul M. Kulesa [a,d,*]

[a] Stowers Institute for Medical Research, 1000 E. 50th St., Kansas City, MO 64110, USA
[b] University of Oxford, Wolfson Centre for Mathematical Biology, Mathematical Institute, Andrew Wiles Building, Radcliffe Observatory Quarter, Woodstock Road, Oxford OX2 6GG, UK
[c] Department of Computer Science, University of Oxford, Oxford OX1 3QD, UK
[d] Department of Anatomy and Cell Biology, University of Kansas School of Medicine, Kansas City, KS 66160, USA

ARTICLE INFO

Article history:
Received 3 June 2015
Received in revised form
10 August 2015
Accepted 12 August 2015
Available online 13 August 2015

Keywords:
Neural crest
Chick
Cell migration
Embryonic microenvironment
Gene expression
Molecular profile
Computational modeling
Trailblazers

ABSTRACT

Embryonic neural crest cells travel in discrete streams to precise locations throughout the head and body. We previously showed that cranial neural crest cells respond chemotactically to vascular endothelial growth factor (VEGF) and that cells within the migratory front have distinct behaviors and gene expression. We proposed a cell-induced gradient model in which lead neural crest cells read out directional information from a chemoattractant profile and instruct trailers to follow. In this study, we show that migrating chick neural crest cells do not display distinct lead and trailer gene expression profiles in culture. However, exposure to VEGF in vitro results in the upregulation of a small subset of genes associated with an in vivo lead cell signature. Timed addition and removal of VEGF in culture reveals the changes in neural crest cell gene expression are rapid. A computational model incorporating an integrate-and-switch mechanism between cellular phenotypes predicts migration efficiency is influenced by the timescale of cell behavior switching. To test the model hypothesis that neural crest cellular phenotypes respond to changes in the VEGF chemoattractant profile, we presented ectopic sources of VEGF to the trailer neural crest cell subpopulation and show diverted cell trajectories and stream alterations consistent with model predictions. Gene profiling of trailer cells that diverted and encountered VEGF revealed upregulation of a subset of 'lead' genes. Injection of neuropilin1 (Np1)-Fc into the trailer subpopulation or electroporation of VEGF morpholino to reduce VEGF signaling failed to alter trailer neural crest cell trajectories, suggesting trailers do not require VEGF to maintain coordinated migration. These results indicate that VEGF is one of the signals that establishes lead cell identity and its chemoattractant profile is critical to neural crest cell migration.

1. . Introduction

One of the most striking examples of embryonic cell migration is the multipotent, highly invasive neural crest. Neural crest cells exit the dorsal neural tube in a rostral-to-caudal order and are sculpted into discrete streams that travel throughout the landscape of the developing vertebrate embryo (Theveneau and Mayor, 2012; Kulesa and McLennan, 2015). Neural crest migration distributes cells to nearly every major organ. As such, a large class of neural-crest-related congenital birth defects has been termed neurocristopathies (Cordero et al., 2011; McKeown et al., 2013; Butler Tjaden and Trainor, 2013; Kulesa et al., 2013). Neurocristopathies may severely affect craniofacial, cardiovascular and autonomic nervous system function. In addition, neural-crest-derived melanoma and neuroblastoma can be very aggressive cancers (Kulesa et al., 2013; Maguire et al., 2015). Thus, the invasive ability and significant contribution to organogenesis of the neural crest make this cell population an important model of study in development and cancer.

Advances in time-lapse imaging in a number of embryo model systems have revealed the complexity of neural crest migratory

* Corresponding author at: Stowers Institute for Medical Research, 1000 E. 50th St., Kansas City, MO 64110, USA.
E-mail address: pmk@stowers.org (P.M. Kulesa).
[1] Both authors contributed equally to this work.

http://dx.doi.org/10.1016/j.ydbio.2015.08.011
0012-1606/

patterns (Blasky et al., 2014; Clay and Halloran, 2014; McGurk et al., 2014; Moosmann et al., 2014; Kulesa et al., 2013; Nishiyama et al., 2012). Neural crest cells may move collectively in sheets and chains, or as individuals in multicellular streams (McLennan and Kulesa, 2015). Regardless of the type of migration, neural crest cells follow stereotypical migratory pathways during prolonged movements to the periphery (persistence). Individual cell trajectories tend to be directed (linearity) within streams that maintain a discrete integrity (cohesion). Thus, despite the wide variety of neural crest cellular phenomena, there are common features of neural crest cell migratory patterns that include persistence, linearity and cohesion.

To more rapidly test hypothetical mechanisms of neural crest cell persistence, linearity, and stream cohesion, computational models have been formulated from empirical data. These models include: (1) frontal expansion (Newgreen et al., 2013); (2) co-attraction/contact inhibition of locomotion (CIL) (Carmona-Fontaine et al., 2011) and; (3) cell-induced gradient (McLennan et al., 2012). The frontal expansion model is based on enteric neural crest cell dispersion and proliferation within open spaces of the developing gut (Young et al., 2004; Simpson et al., 2007). Time-lapse imaging of mouse enteric neural crest cells has revealed that advancing cells move with low directionality and are leap-frogged by trailer cells in a repeating pattern (Young et al., 2014). In contrast, the co-attraction and contact inhibition of locomotion (CIL) model proposes that secretion of a local chemoattractant by migrating neural crest cells prevents widespread dispersal and makes CIL more efficient to generate cell polarity and directed movement (Carmona-Fontaine et al., 2011; Woods et al., 2014). Lastly, we proposed a cell-induced gradient model in which lead neural crest cells respond to a chemotactic guidance signal and instruct trailer cells to follow (McLennan et al., 2012, 2015). Together, these models that reflect the diverse characteristics of neural crest cell migratory patterns throughout the embryo are helping to shed light on underlying mechanisms.

The discoveries that chemotactic factors are present within the embryonic microenvironment changed the neural crest cell migration paradigm. These chemotactic factors include glial cell derived neurotrophic factor (GDNF) (Lake and Heuckeroth, 2013), platelet derived growth factor (PDGF) (Eberhart et al., 2008; He and Soriano, 2013), fibroblast growth factors (FGFs) (Sato et al., 2011) and vascular endothelial derived growth factor (VEGF) (McLennan et al., 2010), complement fragment c3a (Carmona-Fontaine et al., 2011), and stromal cell-derived factor 1 (SDF1) (Kasemeier-Kulesa et al., 2010; Saito et al., 2012; Theveneau et al., 2013). This evidence has led to questions about how neural crest cells interpret chemical signals both in their microenvironment and from/to each other to move in a directed manner and migrate as a coordinated population.

We previously showed that VEGF acts as a chemoattractant for neuropilin-1 expressing cranial neural crest cells in chick (McLennan et al., 2010). Loss of neuropilin-1 function caused neural crest cells to stop prior to entering the second branchial arch (McLennan and Kulesa, 2007). Computational modeling then predicted the presence of lead and trailer neural crest cells in the presence of a VEGF chemoattractant profile shaped by tissue growth and cell consumption, which we termed a cell-induced gradient model (McLennan et al., 2012). Gene profiling identified distinct expression patterns between lead and trailer neural crest cells (McLennan et al., 2012) that correlated with unique cell behaviors observed within each of these two subpopulations (Teddy and Kulesa, 2004). Tissue transplantations that placed trailer neural crest cells in advance of the leaders showed trailers adopted invasive behaviors and gene expression based on their new stream position (McLennan et al., 2012). Further single-cell profiling has now identified a stable and consistent molecular signature unique to a subset of lead cells narrowly confined to the advancing migratory front, which we call trailblazers (McLennan et al., 2015). Whether VEGF is one of the microenvironmental signals that establishes lead and trailer neural crest cell identities, and how cells interpret the VEGF chemoattractant profile to move in a directed manner, remains unknown.

Here, we study these questions using the chick embryo model system and agent-based computational modeling. We first compare the gene expression profiles of migrating neural crest cells exiting from neural tube explant cultures to in vivo data. We examine the response of neural crest gene expression to timed addition and removal of VEGF in this assay. Based on these data, we implement an integrate-and-switch mechanism into our computational model and test cell migration efficiency as a function of switching times. To test the neural crest migratory response to alterations in the in vivo VEGF chemoattractant profile, we place ectopic sources of VEGF either adjacent or within the trailer portion of the stream and monitor alterations to cell trajectories, stream integrity, and gene expression. We test whether trailer neural crest cells require VEGF for guidance by morpholino knockdown of VEGF production in the ectoderm or by binding endogenous VEGF protein within the migratory pathway. Finally, we examine changes in lead neural crest cell gene expression in response to reduction in VEGF signaling either by binding up of endogenous VEGF or knockdown of the neuropilin1 receptor by siRNA.

2. Materials and methods

2.1. Embryos, in ovo cell labeling and tissue transplantation

Fertilized white leghorn chicken eggs (supplied by Centurion Poultry Inc., Lexington, GA) were incubated at 38 °C in a humidified incubator until the desired HH (Hamburger and Hamilton, 1951) stage of development.

For VEGF transplant experiments, premigratory neural crest were labeled by injecting Vybrant DiO (V22889, Invitrogen, Carlsbad, CA) into the lumen of the neural tube. Embryos were then re-incubated for 12 h to allow neural crest cells to exit the neural tube and form a discrete migratory stream. Clumps of DiI-labeled endothelial cells (control (CRL-2279, ATCC, Manassas, VA)) or VEGF-expressing cells (CRL-2460, ATCC) grown as hanging drop cultures were then transplanted either within or adjacent to the trailer subpopulation of the migrating neural crest stream. Manipulated embryos were either re-incubated for 1 h and then mounted on glass bottom dishes (P35G-1.5-20-C, MatTek Corporation, Ashland, MA) for time-lapse imaging as previously described (Chapman et al., 2001; McKinney et al., 2013) or for 12 h before being harvested for static imaging and cell isolation for gene expression profiling as previously described (McLennan et al., 2012). For VEGF signaling knockdown experiments, neuropilin-1-Fc (566-NNS, R&D Systems, Inc.) targeted injections and neuropilin-1 siRNA electroporations were performed as previously described (Bron et al., 2004; McLennan and Kulesa, 2007). Control GFP (pMES) or fluorescently tagged VEGF morpholino (GeneTools, Philomath, OR) was targeted to the ectoderm directly overlying the trailer neural crest cell subpopulation by injecting a small amount of construct or morpholino immediately above the cranial ectoderm on one side of the embryo at HH St 9-11, and then electroporated with platinum electrodes placed on either side of the embryo. After 24 h re-incubation, embryos were fixed, cryostat sectioned and HNK-1 immunohistochemistry was performed as previously described (McLennan et al., 2010).

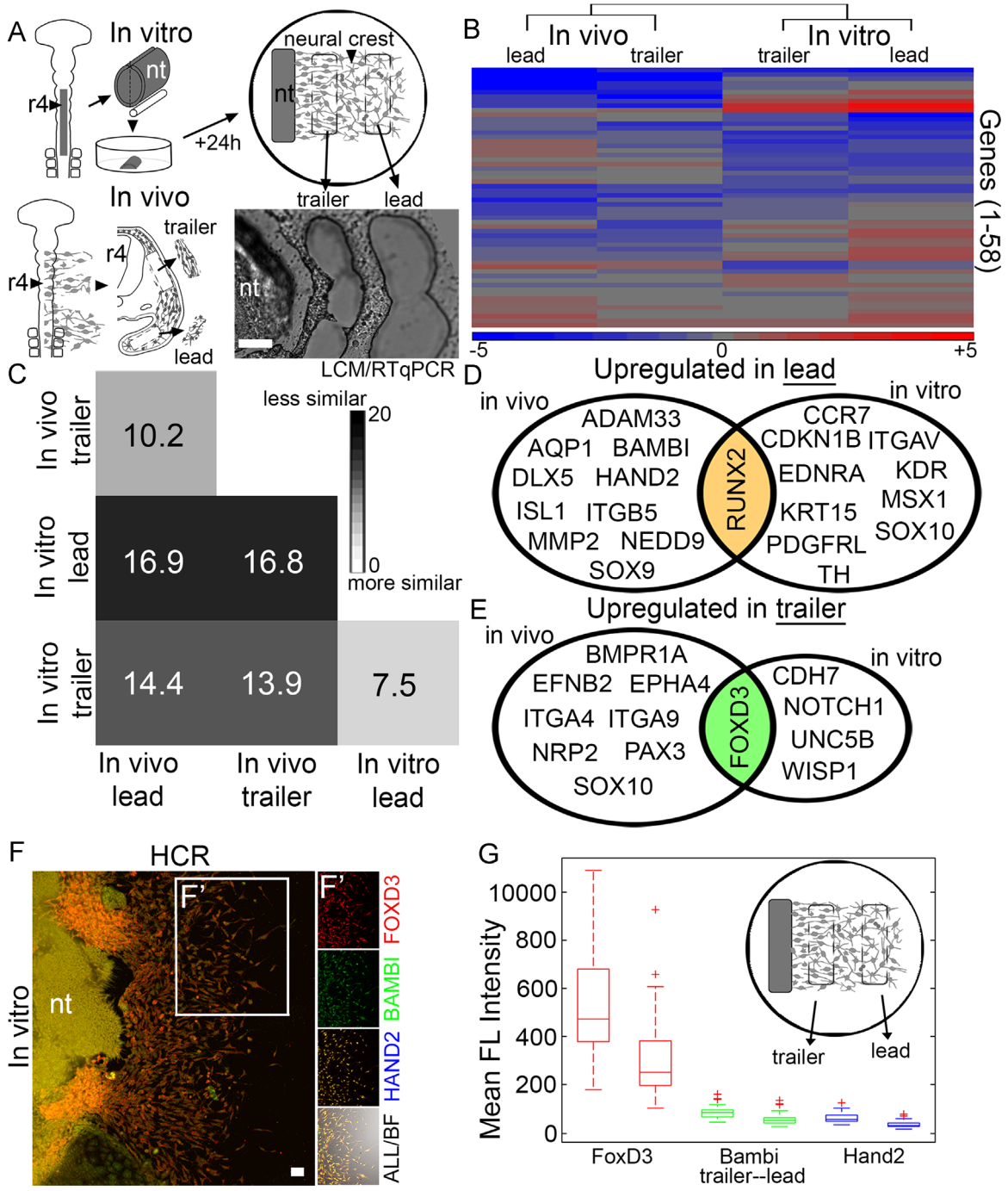

Fig. 1. Neural crest cells do not maintain lead and trailing molecular profiles in vitro. (A) Schematic of in vitro and in vivo neural crest isolation from trailer and lead regions. (B–C) Euclidean clustering and dissimilarity matrix plot of trailer and lead molecular profiles isolated from in vitro and in vivo samples. (D) Venn diagram of genes significantly upregulated in lead neural crest cells. (E) Venn diagram of genes significantly upregulated in trailer neural crest cells. (F) HCR of neural crest cells grown in vitro, probed for FOXD3, HAND2 and BAMBI. (F′) Inset of the subregion outlined in (F); the gain in BAMBI and HAND2 images has been increased post-processing to visualize the cells since the fluorescence signal is low. (G) Mean fluorescence intensity of the HCR probes. nt, neural tube, r4, rhomobomere 4, 24 h, 24 hours, LCM, laser capture microdissection, RTqPCR, reverse transcription quantitative polymerase chain reaction, FL, fluorescence.

2.2. *In vitro assays*

Cranial neural tubes (r2-r6) containing premigratory neural crest cells were cultured in vitro as previously described (McLennan et al., 2010). For the lead/trailer molecular analysis, neural tubes were plated on nuclease-free 1.0 PEN Membrane Slides (415190-9081-000, Zeiss, Jena, Germany) so that neural crest cells would migrate onto the slides and be easily and selectively isolated. After 24 h of incubation to allow for neural crest migration, slides were dehydrated with 100% ethanol for 5 min. Using a PALM Microbeam (Zeiss), neural crest cells adjacent to the neural tube (trailers) and at the edge of the invasive front (leaders) were catapulted without contact into an adhesive cap (415190-9181-000, Zeiss), lysed and used for RT-qPCR on an ABI 7900HT Fast Real-Time PCR system (ABI, Oyster Bay, NY). For the time-course exposure to VEGF, neural tubes were plated on glass bottom dishes, one neural tube per dish (3 dishes/replicates per condition/time point). After overnight incubation, with Ham's F-12 Nutrient Mix Media (11765054, Invitrogen, Grand Island, NY), neural tubes were removed leaving only neural crest cells. Ham's F-12 Nutrient Mix

Media containing VEGF then replaced the plain media for 2 h, and then the media was replaced with plain media for 1.5 h(Fig. 3A). This media was then replaced with media containing VEGF cells were harvested for expression analysis at different times (Fig. 3A). Neural crest cells were lysed directly on the glass bottom dishes at different time points by replacing media with 10 ul of Cells-to-Ct lysis solution containing 1:100 DNAse I (4387299, Life Technologies-Invitrogen). The lysis reaction was halted, after 15 min at room temperature, with 1 ul of Stop solution and samples were immediately placed on dry ice and stored at −80 °C.

2.3. Molecular profiling

cDNA was synthesized directly from sample lysates (438814, Life Technologies) in reactions that included 1 ul of RNAse inhibitor (N261b, Promega, Madison, WI). Gene-specific targets were pre-amplified from a portion of the cDNA in 20 ul preamp reactions using 14 thermal cycles according to a miniaturized version of Life Technologies' Cells-to-Ct preamp kit (4387299, Life Technologies). Pre-amplified products were diluted with 1X TE before being analyzed by microfluidic RT-qPCR on Fluidigm's Biomark HD platform. Non-logarithmic curves were manually removed in Biomark software. Data were normalized using three reference genes chosen from at least six candidates and analyzed with Biogazelle's qBASE software. To combat the variability inherent within our model system, we set statistical significance at $p < 0.1$, choosing to include rather than exclude potential genes of interest. In lieu of multiple testing correction to eliminate potential false positives, we focused on genes that were implicated consistently in multiple analyses. Partek's Genomics Suite was employed for generating clusters, dissimilarity matrices and intensity plots.

2.4. Fluorescent in-situ hybridization chain reaction (HCR) mRNA expression analysis

Neural tubes were isolated and plated, 5–6 neural tubes per glass bottom dish and incubated overnight as described above. Cultures were fixed in 4% paraformaldehyde at room temperature for 1 h and dehydrated stepwise with an ethanol/PBS-T gradient. Cultures were left overnight in ethanol and then rehydrated stepwise into PBS-T. FoxD3, Hand2 and Bambi mRNA transcripts were visualized simultaneously in neural crest cells in culture dishes placed on the confocal microscope stage and images collected using the same imaging settings for all cultures (LSM 710, Zeiss). HCR probes were used at a concentration of 2 nM and hairpins at a concentration of 30 nM.

2.5. Analysis of HCR fluorescence and neural crest cell behaviors

We calculated the intensity of HCR fluorescence in neural tube explant cultures as a measure of gene expression signal. For this analysis, regions of interest were identified either trailer or lead from each explanted neural tube (Fig. 1F). Within the regions of interest, we used the 'Surfaces' function of Imaris (Bitplane USA) to identify cells using the FoxD3 channel and then measured the mean intensity of all fluorescent channels within each surface. The box plots in Fig. 1F were generated by combining the mean intensities from all of the trailer or lead regions of interest. Plus signs indicate outliers, while the box plots and whiskers indicate the quartiles and range, respectively, of each data set.

2.6. Computational modeling

To verify that our experimental observations are consistent with our hypotheses, we employ the hybrid computational model first described in McLennan et al. (2012), with agent-based representation of cells and a chemoattractant described by a continuous reaction-diffusion equation. Previously, we introduced modifications and improvements to the model (McLennan et al., 2015), which we further build upon in this work. For the integrate-and-switch mechanism, we introduced a variable that records how much signal each cell has sensed. This variable increases at a fixed rate when a chemoattractant gradient above the sensing accuracy threshold is sensed, and decreases otherwise, at rates inversely proportional to the parameters leader-to-trailer switching time, t_{LT}, and trailer-to-leader switching time, t_{TL}, respectively. Pseudocode and a table of parameters used can be found in the supplementary materials (Supplementary model information).

To represent transplants of ectopic VEGF, we altered the chemoattractant distribution in our model simulations. From $t = 12$ h (6 h after the start of migration), the background chemoattractant production was increased in a subregion of the migratory domain. To represent placement of a VEGF source outside of the domain (adjacent to the stream), the chemoattractant production was increased in a thin strip of 1/20th the width of the domain, and for placement within the stream, a region of half the domain-width was chosen. In both cases, the length of the transplant was 1/8th of the domain length, and the absolute length increased with domain growth.

3. Results

3.1. Lead and trailer molecular profiles vary according to the embryonic microenvironment and do not exist in vitro

Using morphometric analysis and molecular profiling, we have previously shown that neural crest cells display different phenotypes and gene expression profiles that depend on position within a migratory stream: in particular, a stream is composed of at least two subpopulations, leaders and trailers (McLennan et al., 2012, 2015; Teddy and Kulesa, 2004). Here, we conducted experiments where, as far as possible, the influence of the microenvironment was removed to address whether these subpopulations are predetermined or regulated by the surrounding embryonic microenvironment. We excised neural tubes containing premigratory neural crest cells, allowed the neural crest cells to migrate out from the neural tubes in vitro and isolated cells from the invasive front (lead) and near the neural tube (trailer) to perform molecular profiling (Fig. 1A and Table 1). Euclidean clustering showed that lead and trailer molecular profiles seen in vivo are drastically different to those seen in vitro (Fig. 1B). A Euclidean dissimilarity matrix intensity plot shows that in vitro trail and in vitro lead were the most similar to each other, while in vitro lead and in vivo lead were the least similar to one another (Fig. 1C).

When the molecular profiles were compared at the individual gene level, for each in vivo and in vitro, there were 11/58 genes that were upregulated in the lead, but only one gene that was common, RUNX2 (Fig. 1D). There were 9/58 genes upregulated in the trail in vivo and 5/58 genes upregulated in the trail in vitro but only one gene, FOXD3, that was expressed at high levels in both (Fig. 1E). Thus, even though there were gene expression profile differences in vitro between cells at the invasive front compared to cells near the explanted neural tube, these profiles did not reflect the lead and trailer neural crest cell gene expression profiles we determined in vivo (McLennan et al., 2012).

To confirm our in vitro profiling results by expression analysis, we used fluorescent in-situ hybridization chain reaction (HCR) methodology to simultaneously observe HAND2, BAMBI, and FOXD3 in migrating neural crest cells (Fig. 1F). We found that FOXD3 was strongly expressed in migrating cells near the explanted neural tubes (Fig. 1G, red). In contrast, expression of HAND2 and

Table 1
Genes profiled for in vitro versus in vivo experiments.

Actb	Fgfr1	Notch1
Adam10	Fgfr2	Nrg1
Adam33	Foxd3	Nrp1
Ankk1	Gapdh	Nrp2
Aqp1	Gpc3	Pax3
Bambi	Hand2	Pcdh10
Bmpr1a	Hprt	Pcdh19
Bmpr1b	Isl1	Rplp0
Ccr9	Itga1	Sfrp1
Cdh2	Itga6	Slit2
Cdh6	Itga9	Snail1
Cdh7	Itgb1	Snail2
Cfc1b	Itgb3	Sox10
Ctnnb1	Jag1	Sox9
Cxcr1	Kdr	Tbp
Cxcr4	Krt19	Tfap2a
Ednra	Msx1	Tgfbr1
Efnb2	Nefm	Unc5b
Elav4	Nestin	Ywhaz
Epha4		

BAMBI was very low throughout the entire migrating neural crest cells in vitro compared to in vivo (Fig. 1G, blue and green boxplots). Therefore, gene expression analyses by HCR agreed with our in vitro RT-qPCR profiling results and confirmed that the in vivo lead/trailer molecular signatures do not exist in vitro.

To investigate whether VEGF could influence the gene expression profile of migrating neural crest cells in culture, we harvested and profiled lead and trailer cells after neural tube cultures were exposed to VEGF for 24 h (Fig. 2A). Euclidean clustering and dissimilarity matrix intensity plots showed that upon exposure to VEGF, lead and trailer gene profiles in vitro were still very different to the lead and trail molecular signatures measured in vivo (Fig. 2B and C). Exposure to VEGF in lead neural crest cells in vitro resulted in significant expression changes of 14 genes examined (Fig. 2D). Of these 14, 9/14 were up- and 5/14 were downregulated, compared to in vitro lead neural crest cells not exposed to VEGF (Fig. 2D). Three of the genes that were upregulated are genes typically associated with the most invasive in vivo lead neural crest cells narrowly confined to the migratory front (termed 'trailblazers' in McLennan et al., 2015); NEDD9, BAMBI and NOTCH1 (Fig. 2D, purple). These results are consistent with the idea that the neural crest microenvironment impacts the lead and trailer neural crest cell identity.

3.2. *Neural crest genes are rapidly induced in vitro in response to changes in VEGF*

We previously showed in vivo that trailer neural crest cells transplanted into the migratory front altered their gene expression profile to correspond with the new stream position, when examined 12 h after transplantation (McLennan et al., 2012). Given these data, we refined our computational model to reflect a lead-to-trailer cell behavioral switch (see Supplementary model information). However, it has remained unclear just how rapidly neural crest cells alter their gene expression in response to changes in the VEGF chemoattractant profile.

To examine this question, we performed a series of timed experiments in which neural tube cultures were grown for 24 h, then exposed to VEGF for 2 h (Fig. 3A). VEGF was then removed and after 90 min was re-applied (Fig. 3A). We anticipated gene expression changes would occur within 90 min of changes to the presence/absence of VEGF in culture since we observed in vivo

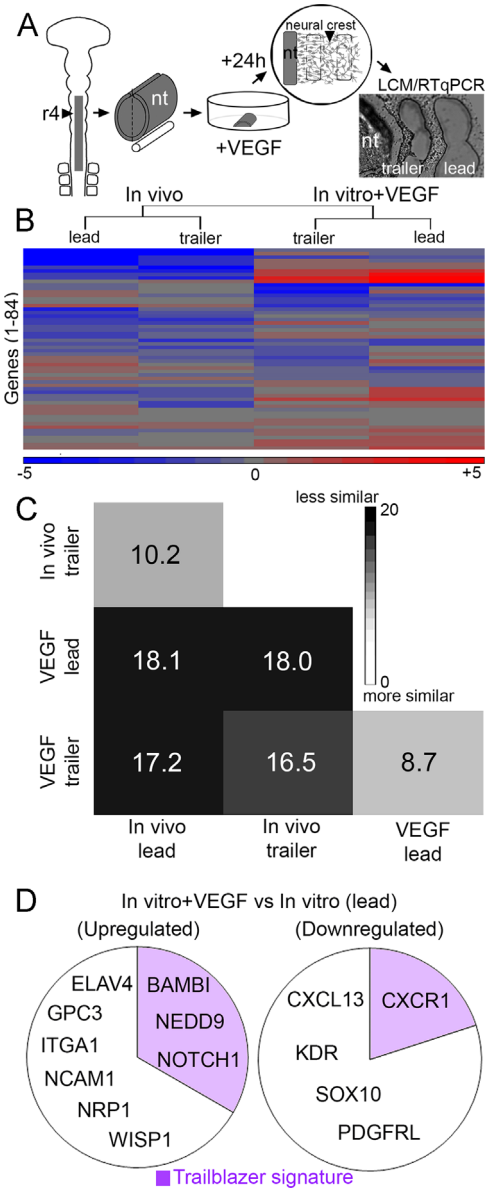

Fig. 2. Neural crest cells upregulate genes typically associated with the migratory invasive front when exposed to VEGF. (A) Schematic of experimental design. (B, C) Euclidean clustering and Euclidean dissimilarity matrix plot of lead and trailer molecular profiles isolated from in vitro samples after addition of VEGF and compared to in vivo samples. (D) Genes significantly upregulated and downregulated in lead in vitro neural crest cells upon exposure to VEGF compared to lead neural crest cells in vitro not exposed to VEGF. Purple highlight indicates genes associated with the neural crest cell trailblazers. nt, neural tube, r4, rhombomere 4, 24 h, 24 hours, LCM, laser capture microdissection, RTqPCR, reverse transcription quantitative polymerase chain reaction.

that trailer neural crest cells diverted trajectories within 1 h after exposure to ectopic VEGF sources (Fig. 6). Samples of migrating neural crest cells for RNA isolation and profiling were taken at a set of non-linearly spaced time points to cover the possible scales of a few minutes to over 1 h (Fig. 3A).

When the temporal expression of all genes was examined (Table 2, 96 total genes analyzed), we found that 17/96 (18%) showed a consistent change in expression within the first 4 min after VEGF removal (Fig. 3B). However, the response times of those same 17 genes varied greatly (within a 1 h window) when VEGF was re-applied (Fig. 3B). We did observe a distinct set of 9/96 (~10%) genes respond rapidly within 4 min after readdition of VEGF (Fig. 3B). Initially, these same 9 genes showed consistent changes in expression

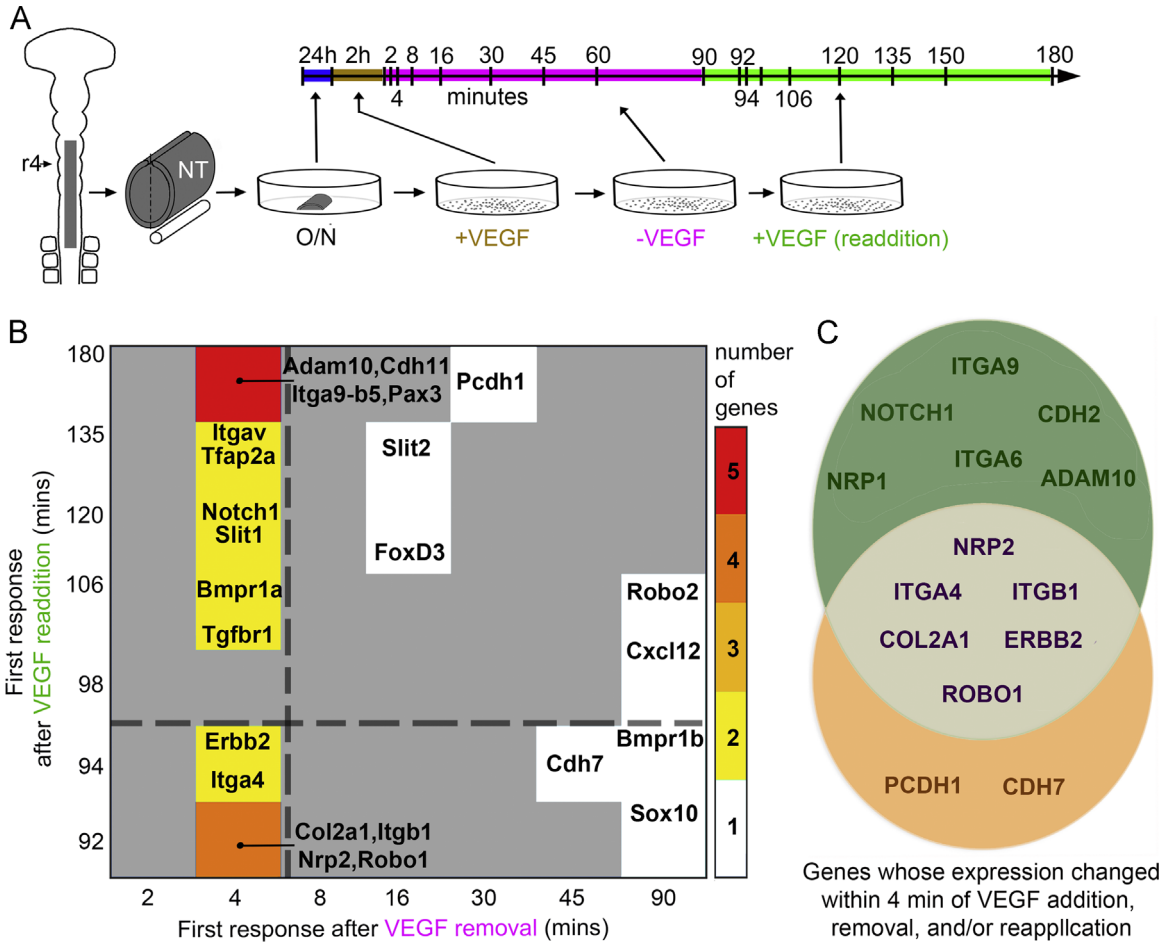

Fig. 3. Response of neural crest cell molecular profiles to removal and readdition of VEGF. (A) Experimental time-course schematic. (B) Summary of first response times of genes that had a significant response (at any time point) after removal (*x*-axis) as well as readdition (*y*-axis) of VEGF ($n=25$ genes). (C) Summary of rapid gene expression changes within the first 4 min of exposure, removal, and/or readdition of VEGF in culture. All genes listed were significantly downregulated within the first 4 min upon exposure to VEGF. Genes shown in green were upregulated within the first 4 min after removal of VEGF, but displayed no significant change within the first 4 min upon the readdition of VEGF. Genes shown in orange displayed no significant change within the first 4 min after removal of VEGF, and were significantly downregulated within the first 4 min upon the readdition of VEGF. Genes shown in the overlap were upregulated within the first 4 min after removal of VEGF, and then significantly downregulated within the first 4 min upon the readdition of VEGF. All genes listed were initially all downregulated upon exposure to VEGF. No genes were upregulated in this diagram upon initial exposure to VEGF. The color coding is then indicating responses during the removal or readdition. r4, rhombomere 4, nt, neural tube.

over a 1 h period after VEGF removal (Fig. 3B). Thus, with either removal or readdition of VEGF to neural tube cultures, we observed very rapid changes in neural crest gene expression profiles.

We also found that after initial exposure to VEGF for two hours, 18 genes were significantly downregulated (Fig. 3C). Of these 18 genes, 14 genes had reoccurring responses to removal and/or readdition of VEGF (Fig. 3C). That is, 6/14 genes were significantly downregulated upon exposure to VEGF, upregulated after removal of VEGF, and displayed no significant change upon the readdition of VEGF (Fig. 3C, green). 2/14 genes were significantly downregulated upon exposure to VEGF, showed no significant change after removal of VEGF, then were significantly downregulated after readdition of VEGF (Fig. 3C, orange). Lastly, a distinct set of 6/14 genes were significantly downregulated upon exposure to VEGF, upregulated after removal of VEGF, and then significantly downregulated upon the readdition of VEGF (Fig. 3C, purple). Thus, there was a set of neural crest genes that showed consistent reoccurring responses to in vitro removal and/or readdition of VEGF.

3.3. Computational model migration efficiency depends on behavior-switching timescales

To explore the sensitivity of our computational model to the rates of switching between leader and trailer behavior, as implemented in the integrate-and-switch mechanism (Fig. 4A), we calculated the average number of cells in the domain at $t=24$ h, relative to the non-switching case (McLennan et al., 2015), for different combinations of lead-to-follow and follow-to-lead switching times (Fig. 4B). Migration efficiency was higher when switching times were similar to each other (Fig. 4C). Outcome variability, measured as the coefficient of variation of cell number, was also lower for matched switching times (Fig. 4C). Migration was least efficient for slow follow-to-lead switching times (Fig. 4B). Together with the in vitro gene expression analysis, which shows fast response to VEGF removal in particular (Fig. 3B) and thus suggests fast lead-to-follow switching, this constrains our model to behavior-switching timescales on the order of a few minutes.

3.4. Trailer neural crest cells respond to ectopic VEGF

We have previously shown that lead neural crest cells can respond to and divert cell trajectories towards ectopic sources of VEGF placed adjacent to the migratory stream within typical cranial neural crest exclusion zones (McLennan et al., 2010). Our model simulations predict that trailer cells receive guidance instructions from leaders, rather than VEGF signals (McLennan et al., 2012). Thus, it has remained unclear whether trailer cells would

Table 2
Genes ($n=96$) profiled for timed response to VEGF.

Adam10	Ephb3	Nrp1
Adam33	Erbb2	Nrp2
Angpt2	Fgf4	Pax3
Ankk1	Fgf8	Pcdh1
Aqp1	Fgfr1	Pcdh19
Bambi	Fgfr2	Pdgfrl
Bmpr1a	Fgfr3	Perp
Bmpr1b	Foxd3	Phox2b
Ccl19	Gpc3	Pkp2
Ccr4	Hand2	Robo1
Ccr5	Il8	Robo2
Ccr7	Isl1	Runx2
Ccr8	Itga1	Slit1
Cdh11	Itga4	Slit2
Cdh2	Itga6	Snail1
Cdh6	Itga9	Sox10
Cdh7	Itgav	Spon1
Cfc1b	Itgb1	Tfap2a
Col2a1	Itgb5	Tgfbr1
Cxcl12	Kdr	Th
Cxcr4	Krt15	Uncb5
Cxcr5	Mbp	Vcam
Dlx5	Mitf	Wisp1
Dsp	Mmp2	Actb
Ednra	Mmp9	Gapdh
Elav4	Msx1	Hprt
Epha1	Ncam2	Rhoa
Epha2	Nedd9	Rplpo
Epha3	Nefm	Ywhaz
Epha4	Notch1	Nes
Epha6	Nrg1	Bdnf
Ephb1	Nrg2	Alk

respond or ignore an ectopic source of VEGF placed within or adjacent to the migratory stream. To address this, we waited until lead neural crest cells had migrated from the neural tube and placed ectopic sources of VEGF either adjacent to or within the trailer subpopulation of the stream (Fig. 5).

When an ectopic VEGF source was placed adjacent to the trailer subpopulation of the neural crest migratory stream, neural crest cells rerouted towards the VEGF source (Fig. 5B compared to Fig. 5A, Movie 1). Neither lead nor trailer neural crest cells were attracted to control cells transplanted into the same region (Fig. 5G; McLennan et al., 2010). Static images suggested that neural crest cells originating from r3 and r4 diverted cell trajectories to move towards the ectopic VEGF source (Fig. 5B). Time-lapse imaging confirmed this and revealed r4 trailer neural crest cells in close proximity to the ectopic VEGF source diverted trajectories (Figs. 6A, B and E).

Supplementary material related to this article can be found online at: http://dx.doi.org/10.1016/j.ydbio.2015.08.011.

From both time-lapse imaging and static analyses we measured on average a small number of trailer neural crest cells leave the migratory stream in response to an ectopic source of VEGF placed adjacent to the trailer portion of the stream (Fig. 5G). However, many trailer neural crest cells that remain confined to the stream tended to cluster near the ectopic VEGF-source (Fig. 6B). This resulted in a change in stream shape such that the width of the stream was significantly increased (Fig. 5H). High resolution time-lapse images of neural crest cells prelabeled with a membrane marker showed that trailer neural crest cells extended multiple filopodial protrusions towards the ectopic VEGF (Fig. 6G; Movie 2). The cells that extended protrusions either broke contact with the VEGF source or moved closer to the source (Movie 2). Lead neural crest cells were unaffected and continued to migrate the entire length of the migratory route (Fig. 5B; Movie 2).

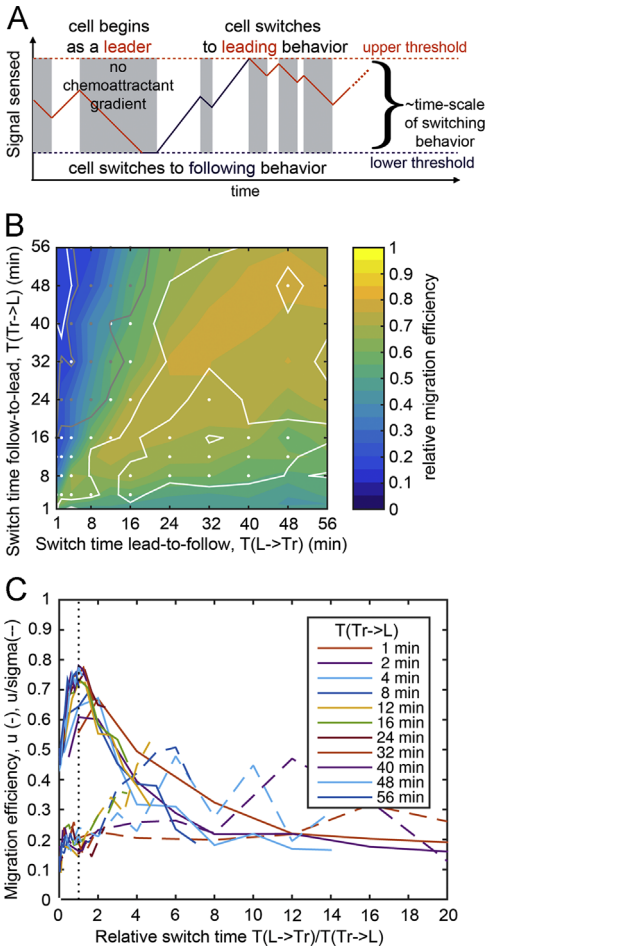

Fig. 4. Model migration efficiency is influenced by behavior-switching timescales. (A) Schematic of integrate-and-switch model for leader-trailer transitions. (B) Effect of switching times on model migration efficiency (defined as the average number of cells after $t=24$ hours ($n=20$ simulations)), relative to the maximum for the non-switching case (as in McLennan et al., 2015). Point spacing indicates parameter combinations sampled. White contours show $>20\%$ coefficient of variation, gray contours $>30\%$. (C) Migration efficiency (solid lines) and coefficient of variation (dashed lines) as a function of the ratio of switching times.

Supplementary material related to this article can be found online at: http://dx.doi.org/10.1016/j.ydbio.2015.08.011.

To determine whether trailer neural crest cells would respond to changes in VEGF signals after receiving hypothetical instructions from leaders, we placed an ectopic VEGF source within the trailer subpopulation of cells (Figs. 5C and 6C compared to 5A; Movie 3). We found that the trailer neural crest cells clustered around the ectopic VEGF source on both the trailer and lead sides of the source (Figs. 5C, 6D and F; Movie 3). The neural crest cells did not treat the tissue transplant as a barrier, since some migrating neural crest cells could be observed to be within the transplant (Figs. 5D, 6D and F). Furthermore, lead neural crest cells were still able to migrate normally the entire length of the migratory route (Fig. 5C). These results reveal that trailer neural crest cells can respond to VEGF, but prefer to remain within their location of the migratory stream.

Supplementary material related to this article can be found online at: http://dx.doi.org/10.1016/j.ydbio.2015.08.011.

3.5. Altering the chemoattractant distribution in model simulations causes break-up of the migratory stream

To test whether the observed effects of transplanting ectopic VEGF could be explained by our model with the integrate-and-

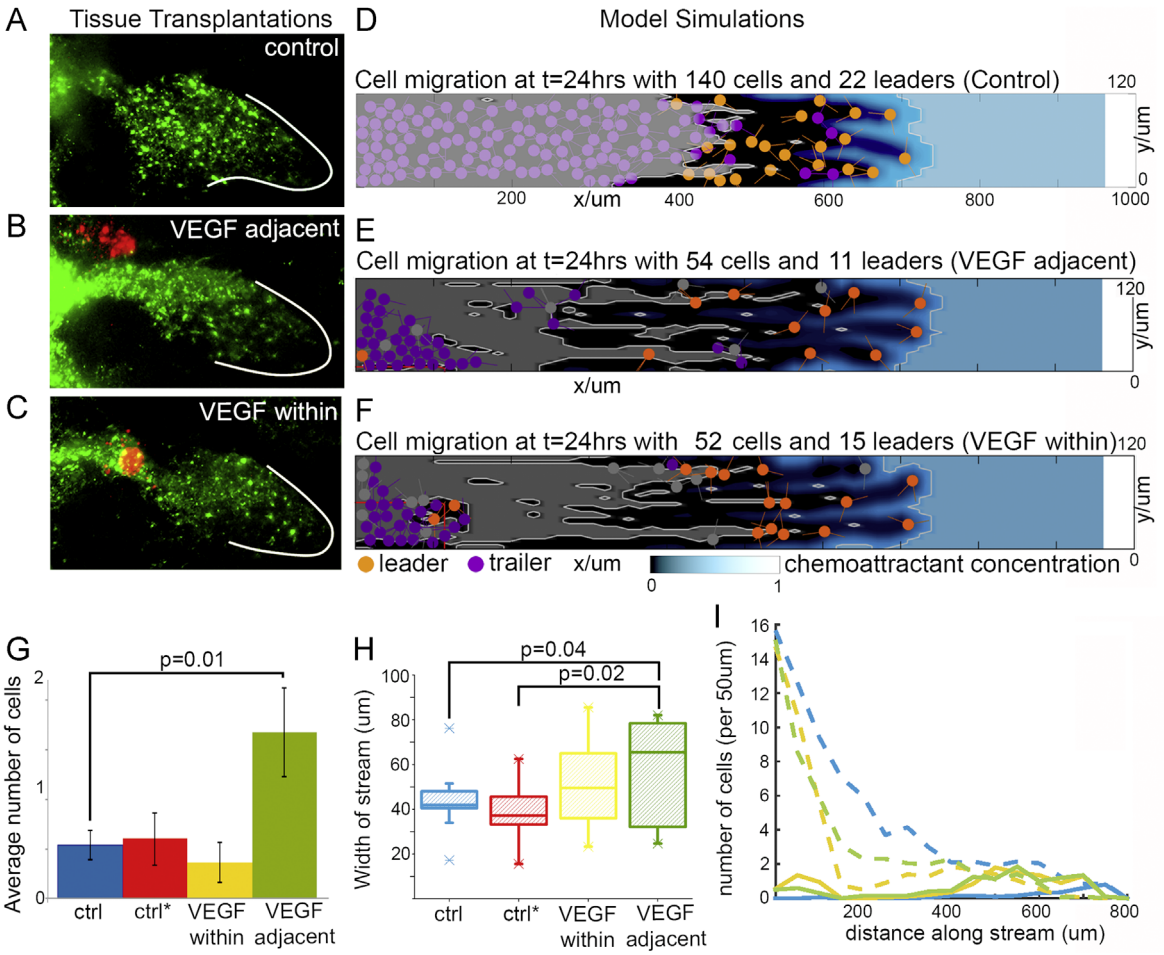

Fig. 5. Trailing neural crest cells respond to VEGF in vivo. (A) Cranial neural crest stream labeled with DiO (green) ($n=18$ embryos). (B) VEGF-expressing cells (red) were transplanted adjacent to trailing portion of the cranial neural crest stream (green) ($n=12$ embryos). (C) Ectopic VEGF cell transplant (red) placed within the trailing portion of the cranial neural crest stream (green) ($n=11$ embryos). (D) Representative control model simulation. (E) Representative model simulation with increased chemoattractant production at bottom left edge of domain from $t=12$ h onwards. (F) Representative model simulation with increased chemoattractant production at bottom left area from $t=12$ hours onwards. (G) Average number of neural crest cells found in area adjacent to r3. (H) Width of the stream at the transplant. Ctrl – control, no transplant, Ctrl* – control, non-VEGF expressing cell transplantation adjacent to stream. (I) Migration profiles of control and perturbed simulations, averaged over $n=20$ simulations. Solid lines=leaders, Dashed lines=trailers. Blue=Ctrl, Gold=VEGF within, Green=VEGF adjacent.

switch mechanism, we computationally represented the tissue transplantation experiments (Fig. 5D–F). In the region of increased chemoattractant production, model simulations showed that trailer cells increasingly switched to become leader cells compared to the control simulations (Fig. 5E and F; Movies 4 and 5). This clustering of cells around the transplants resulted in a break-up of the stream integrity into a lead-moving subpopulation that interacted with the ectopic chemoattractant (Fig. 5E, F and I; Movies 4 and 5). Thus, the effects of perturbing the VEGF distribution in vivo are consistent with our cell-induced gradient model with VEGF-induced cell behavior switching.

Supplementary material related to this article can be found online at http://dx.doi.org/10.1016/j.ydbio.2015.08.011.

3.6. *Trailer neural crest cells near ectopic sources of VEGF upregulate genes associated with trailblazers*

To determine whether the trailer neural crest cells that responded to ectopic sources of VEGF changed their gene expression, we extracted cells by laser capture microdissection (LCM) and performed RT-qPCR analysis on the pooled cells (Fig. 7A). Euclidean clustering revealed that neural crest cells in contact with an ectopic source of VEGF placed within the trailer subregion of the migratory stream were most similar to wildtype trailer neural crest cells (Fig. 7B and C). We found there was a significant upregulation in the expression of nine genes in response to the presence of VEGF (Fig. 7D). This included the expression of four genes (CCR9, CXCR1, PKP2, and BAMBI) (Fig. 7D), which we previously determined to be upregulated in trailblazers (McLennan et al., 2015). Together, this suggested that neural crest cells that encountered an ectopic VEGF source placed within the trailer subpopulation upregulated a subset of trailblazer cell genes but, for the most part, retained similarity to trailer cells.

When neural crest cells diverted away from the typical migratory pathway to encounter an ectopic VEGF source placed adjacent to the stream, we found their gene expression profile changes (Fig. 7B and C). There were 22 genes that were significantly upregulated in the neural crest cells responding to VEGF (Fig. 7E). This list includes eight genes (CCR9, CXCR1, PKP2, BAMBI, CXCR7, NOTCH1, EPHB1 and CTNNB1) that are in the molecular signature of the trailblazers (Fig. 7E, purple). Thus, neural crest cells that diverted away from the discrete stream to interact with an ectopic VEGF source had a higher number of trailblazer genes induced and four of these genes were shared with cells that encounter VEGF within the stream.

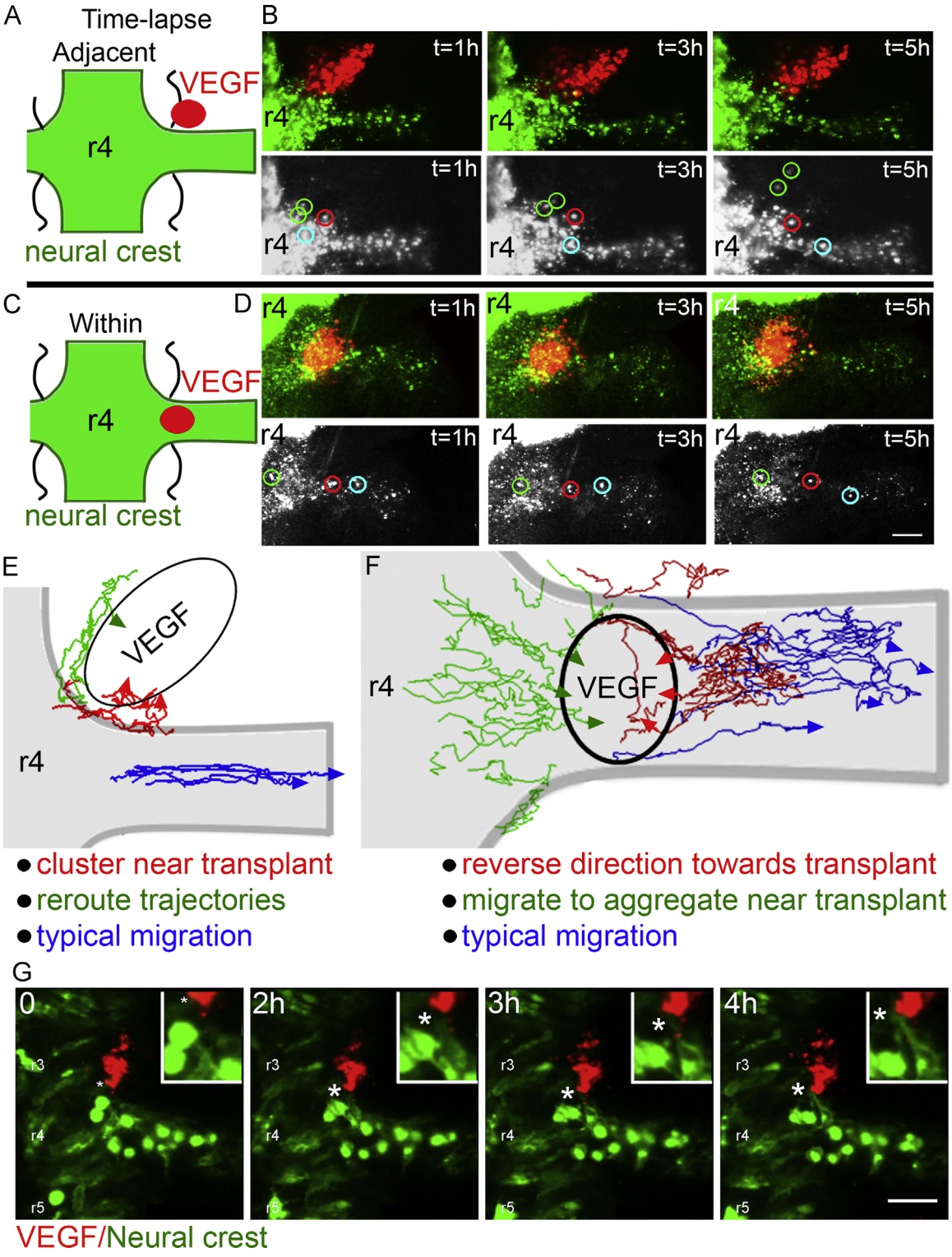

Fig. 6. Trailing neural crest cells reroute towards VEGF in vivo. (A, C) Schematic representations showing placement of the VEGF-expressing cells. (B) Selected images from a typical time-lapse imaging session showing neural crest cells responding to VEGF-expressing cells (red) transplanted adjacent to the trailing stream (green). (D) Selected images from a typical time-lapse imaging session showing neural crest cells responding to VEGF-expressing cells (red) transplanted within the trailing stream (green). (E) Examples of neural crest cell tracks in response to VEGF from time-lapse shown in (B). (F) Examples of neural crest cell tracks in response to VEGF from time-lapse shown in (D). (G) High-resolution image sequence from a typical time-lapse session showing the filopodial dynamics of neural crest cells interacting with an ectopic VEGF sources placed adjacent to the migratory stream. r4, rhombomere 4.

3.7. Trailer neural crest migration is unaffected by a reduction in VEGF signaling

Our hypothesis states that trailer neural crest cells do not require VEGF signaling for guidance, but instead receive guidance instructions from lead cells. To test this, we knocked down VEGF function in the ectoderm directly overlying only the trailer portion of the neural crest migratory stream using targeted VEGF morpholino (Fig. 8A). Knocking down VEGF in the surface ectoderm had no effect on the width of the trailer neural crest cell

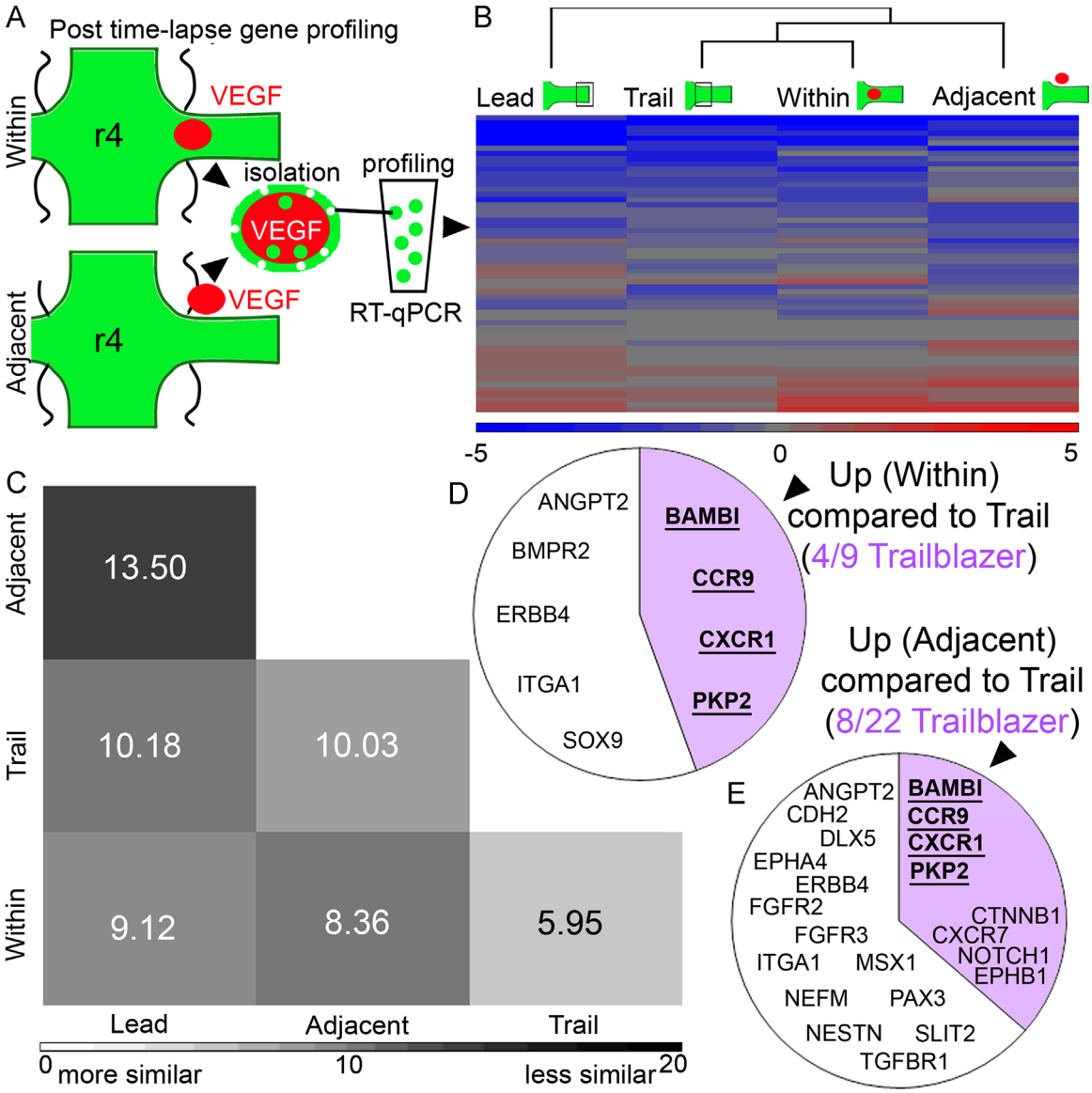

Fig. 7. Trailing neural crest upregulate trailblazer genes in response to ectopic VEGF in vivo. (A) Schematic representation of the experiment. (B–C) Euclidean clustering and Euclidean dissimilarity matrix intensity plot of neural crest cells responding to VEGF. (D, E) Genes significantly upregulated in response to VEGF placed within (D) and adjacent (E). Purple highlight indicates genes typically associated with the neural crest cell trailblazers.

subpopulation when we compared the stream width to control embryos (Fig. 8A). In addition, when we bound up soluble VEGF protein in the trailer mesoderm by injecting Np1-Fc into the tissue, we found no effect to the trailer neural crest subpopulation (Fig. 8B). These results indicated that VEGF is not required for proper migration of the trailer cell population.

3.8. Lead molecular profiles are altered after reduction in VEGF signaling

We have previously shown that Np1 siRNA transfected chick neural crest cells lose cell polarity and stop at the entrance to the second branchial arch (McLennan and Kulesa, 2007). To determine whether a reduction in cellular VEGF signaling significantly influences the molecular profile of lead neural crest cells, we electroporated neural crest cells with Np1 siRNA and isolated these cells for RT-qPCR. We compared the molecular profiles of lead and trailer neural crest cells transfected with Np1 siRNA to lead, middle and trailer neural crest cells transfected with control EGFP. We found that lead Np1 siRNA neural crest cells were most similar in gene expression profile to neural crest cells positioned midstream, rather than leaders (Fig. 9A and C). Trailer Np1 siRNA neural crest cells were most similar to trailer control neural crest cells (Fig. 9A and C).

When we knocked down available VEGF by binding up endogenous VEGF with Np1-Fc injections into and around the migratory stream, we found that lead Np1-Fc neural crest cell molecular profiles were most similar to lead control neural crest cells (Fig. 9B and D). To explain this, it is entirely possible that the microinjection of Np1-Fc into the microenvironment could be diffusely distributed as to be less effective than the Np-1 siRNA in altering cell identity (compare Fig. 9C vs D). Trailer Np1-Fc neural crest cell molecular profiles were most similar to trailer control neural crest cells in agreement with the Np1 siRNA data (Fig. 9B and D), but may also be attributable to less efficient VEGF inhibition.

Comparison of specific genes that were up- or down-regulated in lead neural crest cells after VEGF signaling reduction revealed that lead Np-1 siRNA neural crest cells down-regulated two genes; one of which is associated with typical invasive trailblazers

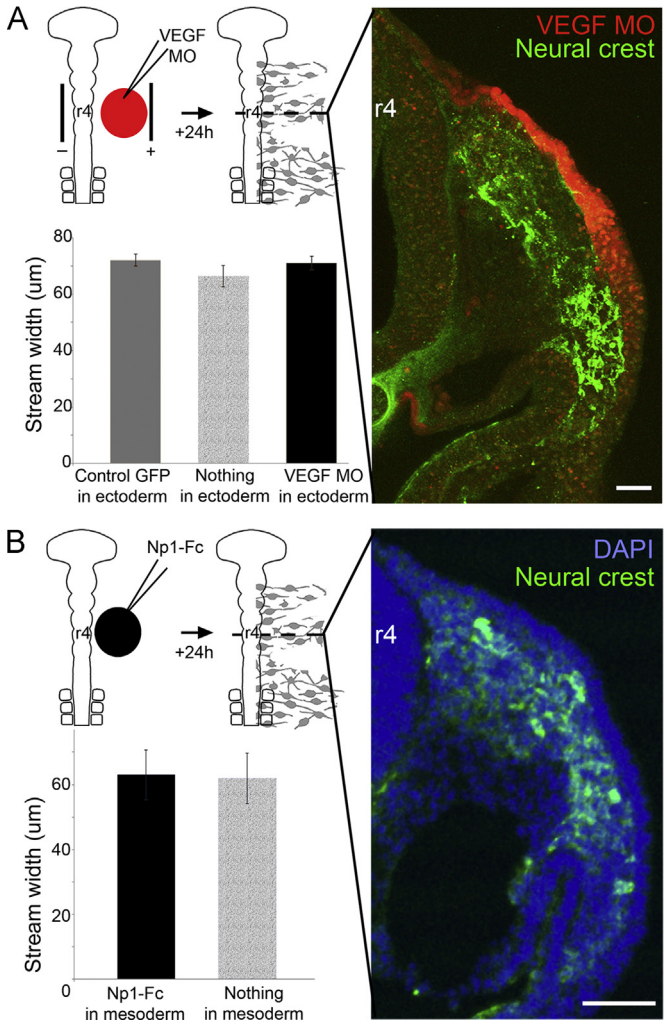

Fig. 8. Trailing neural crest cell migration is not dependent on VEGF. (A) Schematic representation of experimental design of transfecting ectoderm with VEGF morpholino, transverse section of the trailing neural crest migratory stream (green) with VEGF morpholino electroporated into the overlaying ectoderm (red), width of the trailing portion of the migratory stream after ectoderm transfections ($n=9$ embryos for control GFP, 6 embryos for nothing and 8 embryos for VEGF MO). (B) Schematic representation of experimental design of injecting Np1-Fc into the trailing mesenchyme, transverse section of the trailing neural crest migratory stream (green) after Np1-Fc injection, width of the trailing portion of the migratory stream after Np1-Fc injections ($n=5$ embryos). r4, rhombomere 4, MO, morpholino.

(Fig. 9E). There were 11 up-regulated genes, four of which are associated with the trailblazers (Fig. 9E), suggesting cells may respond to other signals for guidance. In comparison, Np1-Fc injections resulted in only one up-regulated gene and eight down-regulated genes in lead cells, four of which are associated with the trailblazer signature (Fig. 9E). Together, these data show that knockdown of VEGF signaling by two distinct methods alters the expression profile in lead neural crest cells and support our previous speculation that loss of neural crest cell polarity and motility (McLennan and Kulesa, 2010) affects gene expression.

4. Discussion

We used the chick embryo system and computational modeling to study the importance of VEGF during neural crest cell migration in the head. We demonstrated that distinct gene expression profiles of lead and trailer neural crest cells do not exist in vitro. However, exposure to VEGF in culture caused an upregulation of a small subset of trailblazer genes. Further, timed addition and removal of VEGF in culture showed neural crest gene expression profiles change within minutes and provided the basis for incorporation of an integrate-and-switch mechanism into our computational model. Model simulations predict that migration efficiency is influenced by lead-to-trailer behavior-switching timescales. We also showed that presentation of ectopic VEGF sources to trailer cells altered cell trajectories and gene expression, consistent with in silico predictions, but loss of VEGF signals in the trailer region did not. We conclude that microenvironmental signals, including VEGF, impact the lead neural crest cell identity.

Signals within the in vivo microenvironment, rather than from the neural tube, establish distinct lead and trailer neural crest cell molecular signatures in the head. By analyzing gene expression in cranial neural crest cells that emigrated from neural tube explant cultures (Fig. 1 and Table 1), we found no evidence of either a trailblazer (McLennan et al., 2015) or lead cell signature (McLennan et al., 2012). Rather, neural crest cell gene expression profiles were independent of the distance migrated in the culture dish (Fig. 1). mRNA expression analysis followed by quantitation of fluorescence signals in individual migrating neural crest cells confirmed the lack of expression of key genes previously correlated with in vivo leaders (Fig. 1F and G). The only exception to this was Runx2 (upregulated in leaders) and FoxD3 (upregulated in trailers), suggesting that the expression of these two genes may be endowed by signals from the neural tube (Fig. 1B–D). If lead/trailer cell phenotypes are not required in vitro, how does directional cell migration away from the neural tube explant occur? Previous in vitro experiments have shown that neural crest cells migrate twice as fast towards explanted ba2 tissue and with twice the directionality than towards control PBS-soaked beads (McLennan et al., 2010). Thus, it can be argued that neural crest cell migration away from neural tube explants is more diffusive than directional.

Exposure of neural tube explant cultures to VEGF partially recovered the expression of genes associated with in vivo lead neural crest cells, including three trailblazer genes (Fig. 2; Bambi, Notch1, and Nedd9; McLennan et al., 2015). This suggested that VEGF may be one of the in vivo microenvironmental signals that establish a distinct trailblazer neural crest cell molecular signature. Of these trailblazer genes, elevated expression of Nedd9 has been associated with metastatic activity in several aggressive cancers (Li et al., 2014; Zhang et al., 2014; Wang et al., 2014). Nedd9 has been shown to be critical to cancer cell invasion due to its ability to stimulate cells to undergo an epithelial-to-mesenchymal transition, attachment to the extracellular matrix and migratory speed, when analyzed in vitro (Zhong et al., 2014; Jin et al., 2014; Sima et al., 2013). Further studies of VEGF and the trailblazer genes, including Nedd9, may reveal the interplay between VEGF stimulation and the functional role of these genes in neural crest migration.

Our computational model included a phenotypic switch from lead to trailer cell phenotype, the simulations of which predicted cell migration efficiency is influenced by switching timescales. By analyzing gene expression dynamics after timed addition and removal of VEGF in vitro, we observed a rapid and significant change in neural crest cell gene expression within four minutes (Figs. 3 and 4; Table 2). From these data, we parametrized our newly extended model so that lead cells become trailers after they fail to read out an appropriate level of VEGF over a short number of time steps.

Simulations of our previous model (McLennan et al., 2012) compared to the new integrate-and-switch mechanism identified two model features that made migration more robust to intrinsic variability, such as: (1) a non-zero timescale of switching between leader and trailer cell states; and (2) hysteresis, or a memory,

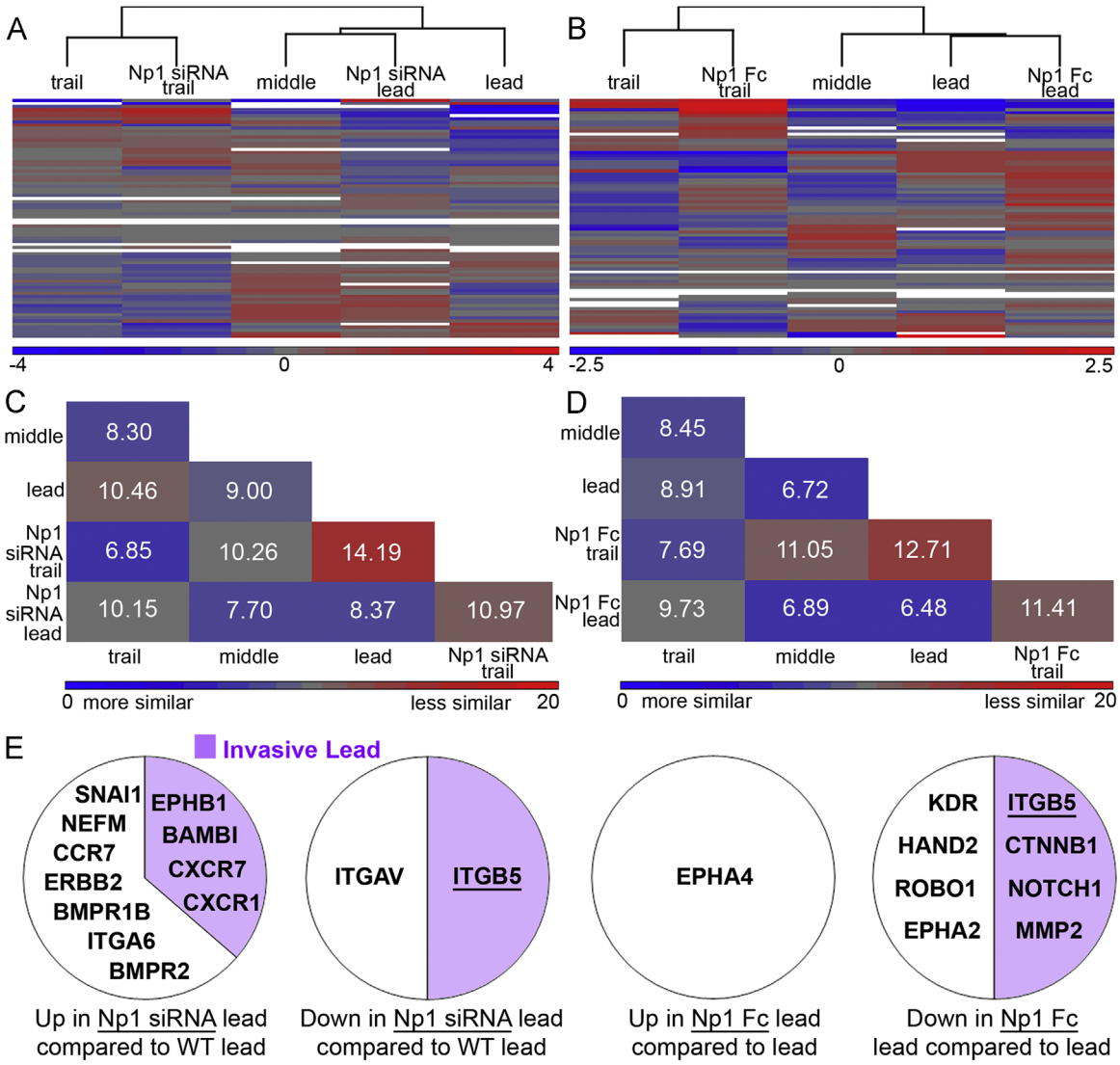

Fig. 9. Lead neural crest cells change their molecular profiles in response to perturbed VEGF signaling. (A, C) Euclidean clustering and Euclidean dissimilarity matrix plot of neural crest cells transfected with Np1 siRNA. (B, D) Euclidean clustering and Euclidean dissimilarity matrix plot of neural crest cells after Np1-Fc injections. (E) Genes significantly altered after VEGF signaling perturbations. Purple highlight indicates genes typically associated with the neural crest cell trailblazers.

which decays with time, of the signal sensed (the directional cue). Thus, the integrate-and-switch mechanism, as presented here, provided the simplest extension to our existing model that captured the plasticity of neural crest cell behavioral identity and did so robustly. It is important to note that the integrate-and-switch mechanism in fact makes our model of neural crest cell migration less complex, in the sense that the size of the lead subpopulation does not need to be pre-specified, but emerges from the interactions of the cells with the chemoattractant distribution.

Trailer neural crest cells altered trajectories and gene expression in response to an ectopic source of VEGF, suggesting the trailer phenotype and gene expression profile are not hard-wired (Movies 1–3). When ectopic VEGF was placed adjacent to the trailer subpopulation (in the region adjacent to r3), some trailer neural crest cells diverted away from the stream towards the ectopic VEGF source (Fig. 6). Diverted trailer cells that encountered the ectopic VEGF source had significant changes in gene expression, including upregulation of 22 genes, 8 of which were trailblazer signature genes (Fig. 7).

Similarly, ectopic VEGF placed within the trailer subpopulation caused newly exiting cells to stop and interact with the VEGF source and cells in front of the ectopic VEGF to reverse direction to move back to the VEGF source (Fig. 6C, D and F; Movie 3). Neural crest cells that encountered ectopic VEGF upregulated nine genes typically associated with the invasive front (Fig. 7). Four trailblazer signature genes were commonly upregulated (Bambi, Ccr9, Cxcr1, and Pkp2) in the ectopic VEGF source transplantations. The chemokine receptors Ccr9 and Cxcr1 have been implicated in aggressive cancers (Johnson-Holiday et al., 2011; Heinrich et al., 2013; Amersi et al., 2008), suggesting correlation with an invasive cell type. VEGF directly stimulated the expression of Cxcr1 and Ccr9 in trailer cells in vivo (Fig. 7), but not in the presence of VEGF in vitro (Fig. 2). Whether the upregulation of Cxcr1 in trailer neural crest cells in response to ectopic VEGF also suggests the presence of the ligand IL8 is unknown. The Cxcr1/Il8 axis has been implicated in a number of invasive cell migration events including mesenchymal stem cell migration to gliomas (Chen et al., 2014) and in neutrophil chemotaxis (Oehlers et al., 2010).

Model simulations predicted that neural crest cells that diverted towards ectopic VEGF sources switched from trailer to leader, resulting in alterations to stream morphology that agreed with experimental results (Fig. 5; Movies 4 and 5). When VEGF was knocked down in either the ectoderm overlaying the trailer portion of the stream (to reduce VEGF production) or the

mesoderm (to bind up existing VEGF protein), there was no effect on trailer neural crest cell migration (Fig. 8). This suggested that VEGF signals are not required for guidance of trailer neural crest cells, which instead may rely on cell contact or unknown microenvironmental signals for guidance.

In summary, our findings identify the importance of VEGF as one of the in vivo microenvironmental signals that establish a distinct subpopulation of lead neural crest cells. VEGF signals do not provide guidance cues to trailer neural crest cells, but convert trailers to lead cells that alter cell trajectories and gene expression when a VEGF source is introduced ectopically within this subpopulation. These data support our cell-induced gradient model in which microenvironmental signals define and direct lead neural crest cells that instruct trailers to follow. We implemented an integrate-and-switch mechanism in silico, through which lead neural crest cells become trailers and vice-versa, with a distinct, rapid timescale of switching to promote model migration efficiency. Together, these steps appear essential to promote neural crest cell persistence and stream cohesion. Further detailed analyses of the cell behaviors and gene expression changes in migrating neural crest cells may help to elucidate the mechanistic underpinnings of which lead cells instruct trailers to follow and of the lead-to-trailer cell conversion.

Acknowledgements

PMK would like to acknowledge kind and generous funding from the Stowers Institute for Medical Research. We also thank members of the BioInformatics, Histology and Molecular Biology core facilities at the Stowers Institute for Medical Research. Fluidigm Biomark HD dynamic arrays were analyzed at the Children's Hospital Boston IDDRC Molecular Genetics facility. LJS would like to acknowledge the UK Engineering and Physical Sciences Research Council (grant number: EP/F500394/1) for funding through a studentship at the Life Science Interface programme of the University of Oxford's Doctoral Training Centre and thank Michael Bentley, Fred Hoffmann, Victoria Hore, Allon Klein and Ben MacArthur for discussions.

Appendix A. Suplementary information

Supplementary data associated with this article can be found in the online version at: http://dx.doi.org/10.1016/j.ydbio.2015.08.011.

References

Amersi, F.F., Terando, A.M., Goto, Y., Scolyer, R.A., Thompson, J.F., Tran, A.N., Faries, M.B., Morton, D.L., Hoon, D.S., 2008. Activation of CCR9/CCL25 in cutaneous melanoma mediates preferential metastasis to the small intestine. Clin. Cancer Res. 14, 638–645.
Blasky, A.J., Pan, L., Moens, C.B., Appel, B., 2014. Pard3 regulates contact between neural crest cells and the timing of Schwann cell differentiation but is not essential for neural crest migration or myelination. Dev. Dyn. 243, 1511–1523.
Bron, R., Eickholt, B.J., Vermeren, M., Fragale, N., Cohen, J., 2004. Functional knockdown of neuropilin-1 in the developing chick nervous system by siRNA hairpins phenocopies genetic ablation in the mouse. Dev. Dyn. 230, 299–308.
Butler Tjaden, N.E., Trainor, P.A., 2013. The developmental etiology and pathogenesis of Hirschsprung disease. Transl. Res. 162, 1–15.
Carmona-Fontaine, C., Theveneau, E., Tzekou, A., Tada, M., Woods, M., Page, K.M., Parsons, M., Lambris, J.D., Mayor, R., 2011. Complement fragment C3a controls mutual cell attraction during collective cell migration. Dev. Cell 21, 1026–1037.
Chapman, S.C., Collignon, J., Schoenwolf, G.C., Lumsden, A., 2001. Improved method for chick whole-embryo culture using a filter paper carrier. Dev. Dyn. 220, 284–289.
Chen, L., Fan, J., Chen, H., Meng, Z., Chen, Z., Wang, P., Liu, L., 2014. The IL-8/CXCR1 axis is associated with cancer stem cell-like properties and correlates with clinical prognosis in human pancreatic cancer cases. Sci. Rep. 4, 5911.
Clay, M.R., Halloran, M.C., 2014. Cadherin 6 promotes neural crest cell detachment via F-actin regulation and influences active Rho distribution during epithelial-to-mesenchymal transition. Development 141, 2506–2515.
Cordero, D.R., Brugmann, S., Chu, Y., Bajpai, R., Jame, M., Helms, J.A., 2011. Cranial neural crest cells on the move: their roles in craniofacial development. Am. J. Med. Genet. A 155A, 270–279.
Eberhart, J.K., He, X., Swartz, M.E., Yan, Y.L., Song, H., Boling, T.C., Kunerth, A.K., Walker, M.B., Kimmel, C.B., Postlethwait, J.H., 2008. MicroRNA Mirn140 modulates Pdgf signaling during palatogenesis. Nat. Genet. 40, 290–298.
Hamburger, V., Hamilton, H.L., 1951. A series of normal stages in the development of the chick embryo. J. Morphol. 88, 49–92.
He, F., Soriano, P., 2013. A critical role for PDGFRalpha signaling in medial nasal process development. PLoS Genet. 9, e1003851.
Heinrich, E.L., Arrington, A.K., Ko, M.E., Luu, C., Lee, W., Lu, J., Kim, J., 2013. Paracrine activation of chemokine receptor CCR9 enhances the invasiveness of pancreatic cancer cells. Cancer Microenviron. 6, 241–245.
Jin, Y., Li, F., Zheng, C., Wang, Y., Fang, Z., Guo, C., Wang, X., Liu, H., Deng, L., Li, C., Wang, H., Chen, H., Feng, Y., Ji, H., 2014. NEDD9 promotes lung cancer metastasis through epithelial-mesenchymal transition. Int. J. Cancer 134, 2294–2304.
Johnson-Holiday, C., Singh, R., Johnson, E., Singh, S., Stockard, C.R., Grizzle, W.E., Lillard Jr., J.W., 2011. CCL25 mediates migration, invasion and matrix metalloproteinase expression by breast cancer cells in a CCR9-dependent fashion. Int. J. Oncol. 38, 1279–1285.
Kasemeier-Kulesa, J.C., McLennan, R., Romine, M.H., Kulesa, P.M., Lefcort, F., 2010. CXCR4 controls ventral migration of sympathetic precursor cells. J. Neurosci. 30, 13078–13088.
Kulesa, P.M., McKinney, M.C., McLennan, R., 2013. Developmental imaging: the avian embryo hatches to the challenge. Birth Defects Res. Part C: Embryo Today 99, 121–133.
Kulesa, P.M., McLennan, R., 2015. Neural crest migration: trailblazing ahead. F1000Prime Rep. 7, 2.
Lake, J.I., Heuckeroth, R.O., 2013. Enteric nervous system development: migration, differentiation, and disease. Am. J. Physiol. Gastrointest. Liver Physiol. 305, G1–24.
Li, P., Zhou, H., Zhu, X., Ma, G., Liu, C., Lin, B., Mao, W., 2014. High expression of NEDD9 predicts adverse outcomes of colorectal cancer patients. Int. J. Clin. Exp. Pathol. 7, 2565–2570.
Maguire, L.H., Thomas, A.R., Goldstein, A.M., 2015. Tumors of the neural crest: Common themes in development and cancer. Dev. Dyn. 244, 311–322.
McGurk, P.D., Lovely, C.B., Eberhart, J.K., 2014. Analyzing craniofacial morphogenesis in zebrafish using 4D confocal microscopy. J. Vis. Exp., e51190.
McKeown, S.J., Wallace, A.S., Anderson, R.B., 2013. Expression and function of cell adhesion molecules during neural crest migration. Dev. Biol. 373, 244–257.
McKinney, M.C., Fukatsu, K., Morrison, J., McLennan, R., Bronner, M.E., Kulesa, P.M., 2013. Evidence for dynamic rearrangements but lack of fate or position restrictions in premigratory avian trunk neural crest. Development 140, 820–830.
McLennan, R., Dyson, L., Prather, K.W., Morrison, J.A., Baker, R.E., Maini, P.K., Kulesa, P.M., 2012. Multiscale mechanisms of cell migration during development: theory and experiment. Development 139, 2935–2944.
McLennan, R., Kulesa, P.M., 2007. In vivo analysis reveals a critical role for neuropilin-1 in cranial neural crest cell migration in chick. Dev. Biol. 301, 227–239.
McLennan, R., Schumacher, L.J., Morrison, J.A., Teddy, J.M., Ridenour, D.A., Box, A.C., Semerad, C.L., Li, H., McDowell, W., Kay, D., Maini, P.K., Baker, R.E., Kulesa, P.M., 2015. Neural crest migration is driven by a few trailblazer cells with a unique molecular signature narrowly confined to the invasive front. Development 142, 2014–2025.
McLennan, R., Teddy, J.M., Kasemeier-Kulesa, J.C., Romine, M.H., Kulesa, P.M., 2010. Vascular endothelial growth factor (VEGF) regulates cranial neural crest migration in vivo. Dev. Biol. 339, 114–125.
Moosmann, J., Ershov, A., Weinhardt, V., Baumbach, T., Prasad, M.S., LaBonne, C., Xiao, X., Kashef, J., Hofmann, R., 2014. Time-lapse X-ray phase-contrast microtomography for in vivo imaging and analysis of morphogenesis. Nat. Protoc. 9, 294–304.
Newgreen, D.F., Dufour, S., Howard, M.J., Landman, K.A., 2013. Simple rules for a "simple" nervous system? Molecular and biomathematical approaches to enteric nervous system formation and malformation. Dev. Biol. 382, 305–319.
Nishiyama, C., Uesaka, T., Manabe, T., Yonekura, Y., Nagasawa, T., Newgreen, D.F., Young, H.M., Enomoto, H., 2012. Trans-mesenteric neural crest cells are the principal source of the colonic enteric nervous system. Nat. Neurosci. 15, 1211–1218.
Oehlers, S.H., Flores, M.V., Hall, C.J., O'Toole, R., Swift, S., Crosier, K.E., Crosier, P.S., 2010. Expression of zebrafish cxcl8 (interleukin-8) and its receptors during development and in response to immune stimulation. Dev. Comp. Immunol. 34, 352–359.
Saito, D., Takase, Y., Murai, H., Takahashi, Y., 2012. The dorsal aorta initiates a molecular cascade that instructs sympatho-adrenal specification. Science 336, 1578–1581.
Sato, A., Scholl, A.M., Kuhn, E.N., Stadt, H.A., Decker, J.R., Pegram, K., Hutson, M.R., Kirby, M.L., 2011. FGF8 signaling is chemotactic for cardiac neural crest cells. Dev. Biol. 354, 18–30.
Sima, N., Cheng, X., Ye, F., Ma, D., Xie, X., Lu, W., 2013. The overexpression of scaffolding protein NEDD9 promotes migration and invasion in cervical cancer via tyrosine phosphorylated FAK and SRC. PLoS One 8, e74594.
Simpson, M.J., Zhang, D.C., Mariani, M., Landman, K.A., Newgreen, D.F., 2007. Cell proliferation drives neural crest cell invasion of the intestine. Dev. Biol. 302, 553–568.

Teddy, J.M., Kulesa, P.M., 2004. In vivo evidence for short- and long-range cell communication in cranial neural crest cells. Development 131, 6141–6151.
Theveneau, E., Mayor, R., 2012. Neural crest delamination and migration: from epithelium-to-mesenchyme transition to collective cell migration. Dev. Biol. 366, 34–54.
Theveneau, E., Steventon, B., Scarpa, E., Garcia, S., Trepat, X., Streit, A., Mayor, R., 2013. Chase-and-run between adjacent cell populations promotes directional collective migration. Nat. Cell Biol. 15, 763–772.
Wang, H., Mu, X., Zhou, S., Zhang, J., Dai, J., Tang, L., Xiao, L., Duan, Z., Jia, L., Chen, S., 2014. NEDD9 overexpression is associated with the progression of and an unfavorable prognosis in epithelial ovarian cancer. Hum. Pathol. 45, 401–408.
Woods, M.L., Carmona-Fontaine, C., Barnes, C.P., Couzin, I.D., Mayor, R., Page, K.M., 2014. Directional collective cell migration emerges as a property of cell interactions. PLoS One 9, e104969.
Young, H.M., Bergner, A.J., Anderson, R.B., Enomoto, H., Milbrandt, J., Newgreen, D. F., Whitington, P.M., 2004. Dynamics of neural crest-derived cell migration in the embryonic mouse gut. Dev. Biol. 270, 455–473.
Young, H.M., Bergner, A.J., Simpson, M.J., McKeown, S.J., Hao, M.M., Anderson, C.R., Enomoto, H., 2014. Colonizing while migrating: how do individual enteric neural crest cells behave? BMC Biol. 12, 23.
Zhang, Q., Wang, H., Ma, Y., Zhang, J., He, X., Ma, J., Zhao, Z.S., 2014. Overexpression of Nedd9 is a prognostic marker of human gastric cancer. Med. Oncol. 31, 33.
Zhong, J., Bach, C.T., Shum, M.S., O'Neill, G.M., 2014. NEDD9 regulates 3D migratory activity independent of the Rac1 morphology switch in glioma and neuroblastoma. Mol. Cancer Res. 12, 264–273.